

Journal of Physical Chemistry and Functional Materials

Home Page of Journal: <https://dergipark.org.tr/jphcfum>



Synthesis, Characterization and Theoretical Anti-Corrosion Study for Substitute Thiazole Contained Cyclobutane Ring

Arzu Etkeser Aktaş¹ , Rebaz Anwar Omer^{2*} , Pelin Koparir³ , Metin Koparir¹

¹ *Firat University Department of Chemistry, Faculty of Science, 23169, Elazig, Turkey*

² *Department of Physics, Faculty of Science & Health, Koya University, Koya KOY45, Kurdistan Region – F.R. Iraq*

³ *Forensic Medicine Institute, Department of Chemistry, Firat University, 23169 Elazig, Turkey*

*Corresponding author: Rebaz Anwar Omer, E-mail: rebaz.anwar@koyauniversity.org

ABSTRACT

This study was synthesized: 1-(4-(3-methyl-3-phenylcyclobutyl)thiazol-2-yl)-3-phenylthiourea and 1-(4-chlorophenyl)-3-(4-(3-methyl-3-phenylcyclobutyl)thiazol-2-yl)thiourea. Fourier-Transform Infrared (FT-IR) spectroscopy and Nuclear Magnetic Resonance (NMR) characterize the molecular formula. Theoretical vibration was computed with Gaussian 09W software, and corrosion inhibiting activity was computed with quantum chemical calculations. Furthermore, the GaussView 5.0 package was used on the B3LYP/6-311G(d,p) method to calculate the energy of the highest occupied molecular orbital (E_{HOMO}), the energy of the lower occupied molecular orbital, energy gap ΔE , dipole moment (μ), and transmitted electrons (ΔN). The molecular properties such as hardness (η), softness (σ), and electronegativity (χ) were calculated based on the results of inhibitor activity. The corrosion inhibiting activities of the derivatives were predicted using quantum chemical calculations. As a result, the corrosion inhibitor behavior can be predicted without an experimental study, show a strong relationship between organic-based corrosion inhibitors and the process's quantum chemical parameters.

ARTICLE INFO

Keywords:

Thiazole

Cyclobutane

Ring

DFT

HOMO-LUMO

Anti-corrosion

Received: 2022-05-26

Accepted: 2022-06-08

ISSN: 2651-3080

DOI: 10.54565/jphcfum.1121687

Introduction

Thiazoles are azole derivatives (which include imidazoles and oxazoles) with the chemical formula C_3H_3NS , with the atoms organized in five aromatic rings [1]. Thiazole has a light yellow liquid with a pyridine-like odor. Thiazoles are utilized to obtain free carbon particles, which react with transition metals to generate a complex [2-4]. Compared to carbon and sulfur atoms, nitrogen atoms in a thiazole have the highest negative charge on the molecular formula [5]. Thiazoles have been shown potential pharmacological properties, such as being the best heterocyclic chemical to start the production of novel medications [6, 7]. It has been targeted by industry because its Schiff base complexes have distinct chemical activities such as catalytic activation [8, 9], photochromic features [10], electrochemical transfer [11], and complex formation for several toxic metals [12]. On the other hand organic compounds, were not used directly due to cost considerations.

For more than a century, Cyclobutans have been recognized as intriguing structural motifs, but they have received far less attention than their homologs [13, 14]. Because of the highly strained ring topologies, the synthesis of cyclobutane rings, particularly stereospecifically, poses significant challenges in synthetic chemistry. Cyclobutanes have increased the structural stability of a wide range of complex natural products, not just artificial molecules [15, 16]. Because of their novel chemical structures and high biological activity, natural products containing cyclobutane are particularly appealing for total synthesis. Because of their proclivity to release inherent strain energies, cyclobutanes readily undergo several ring-opening reactions [17].

For large systems, DFT has a good cost-accuracy ratio, but the calculations are usually prohibitively expensive in terms of computational effort, and it works better for charged systems (e.g., proteins with charged residues) [18-21]. Theoretical computation methodologies have grown in

popularity for theoretical modelling and the design of functional materials such as pharmaceutical substances [22, 23]. Because it interprets inhibitory activity using several quantum chemical features, computational chemistry is a promising tool for identifying corrosion inhibitors [24, 25]. Energy, molecular orbital energy, and atomic charges are three types of quantum chemistry properties frequently used in theoretical corrosion studies. Several parameters, including E_{HOMO} , E_{LUMO} energy, softness, and hardness, are closely related to inhibitor activity [26-30]. Density Function Theory (DFT) has been widely applied to calculate the total electron energy of a molecule based on its electron density [31-33].

Thiazole ring is an electron-rich system that easily forms hydrogen bonds between molecules of different species. Thiazole-containing compounds have been reported to be broad-spectrum inhibitors [34, 35]. For this purpose, two novel compounds (IIIa, b) from the thiazole series containing cyclobutane derivatives with thiourea were synthesized. The chemical structure of the derivatives was determined using FT-IR and NMR, and corrosion inhibitor activity was explained using DFT methods.

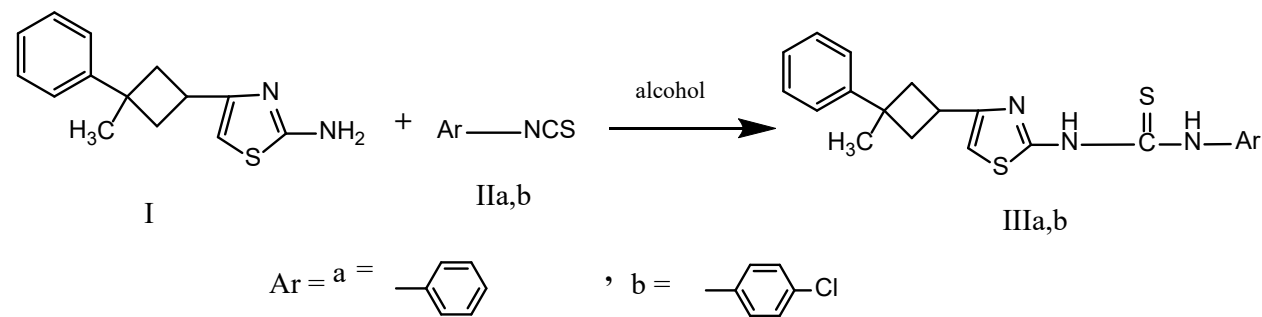


Fig. 1 The methodical approach to synthesizing thiazole derivatives

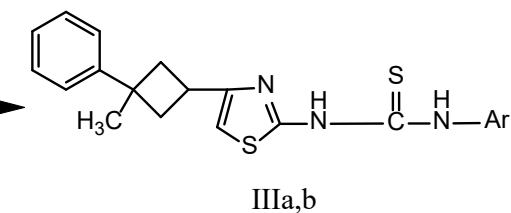
Synthesis 1-(4-(3-methyl-3-phenylcyclobutyl)thiazol-2-yl)-3-phenylthiourea (IIIa)

4-[1-Phenyl-1-Methyl-1-Cyclobutan-3-yl]-2-aminothiazole, 2.44 gm (0.01 mol), CaCl_2 and thermometer were arranged in a 3-mouth reaction flask and thiazole and phenyl isocyanate were calculated (0.01 mol), was placed in the reaction flask. Absolute ethyl alcohol 65 ml was added. The reaction was continued for 1 hour at room temperature. It was refluxed for 12 hours under reflux. The reaction was stopped after observing IR control 3280-320 cm^{-1} NH peak and 1360-1340 cm^{-1} C=S peaks. It was cooled and filtered, the filtrate was washed with water and the ether phase was extracted. It was dried with MgSO_4 , and filtered. The solvent was removed in the evaporator, dissolved in chloroform, precipitated in n-hexane, dried in the open air, and crystallized in ethanol. Yield 63%, Melting point: 274. The molecular characteristics of 1-(4-(3-methyl-3-phenylcyclobutyl)thiazol-2-yl)-3-phenylthiourea (IIIa) summarized below:

IR (cm^{-1} , KBr): (3280-3200) (vN-H), 3107 cycloalkane (vC-H), 3055 Aromatic (vC-H), 2980-2870 Aliphatic (vC-H), 1600-1590 (vC=N), 1360-1340 (vC=S), 1159-1000 (vC-N), 690-655 (vC-S-C). $^1\text{H-NMR}$ (200 MHz, CDCl_3 , ppm, δ), 10.46-10.06 (br, 2H, 2xNH), 7.55-7.12 (m, 10H, Aromatic

Materials and Methods

4-[1-Phenyl-1-Methyl-1-Cyclobutan-3-yl]-2-aminothiazole we got from Firat University organic chemistry Lab. Calcium chloride (CaCl_2) (CAS- 10035-04-8 Istanbul), Thiazole ($\text{C}_3\text{H}_3\text{NS}$) (CAS- 288-47-1 Istanbul), 4-Nitrophenyl isocyanate ($\text{O}_2\text{NC}_6\text{H}_4\text{NCO}$) (CAS- 100-28-7 Istanbul), Ethyl alcohol ($\text{CH}_3\text{CH}_2\text{OH}$) (CAS- 64-17-5 Istanbul), Magnesium sulfate (MgSO_4) (CAS- 7487-88-9 Istanbul), n-Hexane ($\text{CH}_3(\text{CH}_2)_4\text{CH}_3$ Istanbul) (CAS- 110-54-3 Istanbul), 4-Methoxyphenyl isocyanate ($\text{CH}_3\text{OC}_6\text{H}_4\text{NCO}$) (CAS- 5416-93-3 Istanbul). All chemicals were purchased from Merck or Aldrich, and used without further purification. Two new thiazole derivatives of (1-(4-(3-methyl-3-phenylcyclobutyl)thiazol-2-yl)-3-(4-nitrophenyl)thiourea and 1-(4-methoxyphenyl)-3-(4-(3-methyl-3-phenylcyclobutyl)thiazol-2-yl)thiourea synthesized, as shown in Figure 1. The melting point of the derivatives was measured by Gallenkamp digital melting point. ^1H NMR and ^{13}C NMR spectra were recorded on an FX 90 JEOL 200 MHz ^1H NMR and Varian Gemini 100 MHz for ^{13}C , using CDCl_3 as a solvent.



protons), 6.42 (s, 1H, CH=, in thiazole), 3.73-3.60 (p, 1H, methine proton in the Cyclobutane ring), 2.68-2.46 (m, 4H, CH_2 protons in Cyclobutane), 1.56 (s, 3H, CH_3 protons). $^{13}\text{C-NMR}$ (200 MHz, CDCl_3 , ppm), 178.22 (C=S, Cs), 163.11 (C-2 in Thiazole), 157.09 (Aromatic Quaternary C's), 153.81 (C-4 in Thiazole), 140.79, 131.41, 130.30, 127.84, 126.49, 125.47 (Aromatic C's), 106.56 (C-5) in Thiazole, 42.73, 40.93 (Cyclobutane (CH_2)₂ Cs), 32.61, (Cyclobutane CH); 32.03 (CH_3).

Synthesis 1-(4-chlorophenyl)-3-(4-(3-methyl-3-phenylcyclobutyl)thiazol-2-yl)thiourea (IIIb)

4-[1-Phenyl-1-Methyl-1-Cyclobutan-3-yl]-2-aminothiazole, 2.44 g (0.01 mol), CaCl_2 , and thermometer were arranged in a 3-mouth reaction flask, and thiazole and 4-Chlorophenyl isocyanate were calculated (0.01 mol) was placed in the reaction flask. Absolute ethyl alcohol 65 ml was added. The reaction was continued for 1 hour at room temperature. It was refluxed for 12 hours under reflux. After IR control 3280-320 sec NH peak and 1360-1340 C=S peaks were observed, the reaction was stopped. It was cooled and filtered, the filtrate was washed with water and the ether phase was extracted. It was dried with MgSO_4 and filtered. The solvent was removed in the evaporator, dissolved in chloroform, precipitated in n-hexane, dried in the open air,

and crystallized in ethanol. Yield 75%, melting point: 264. The molecular characteristics of 1-(4-chlorophenyl)-3-(4-(3-methyl-3-phenylcyclobutyl)thiazol-2-yl)thiourea (IIIb) summarized below:

IR (cm^{-1} , KBr): 3280-3200 (vN-H), 3107 cycloalkane (vC-H), 3055 Aromatic (vC-H), 2980-2870 Aliphatic (vC-H), 1600-1590 (vC=N), 1360-1340 (vC=S), 1159-1000 (vC-N), 690-655 (vC-S-C). $^1\text{H-NMR}$ (200 MHz, CDCl_3 , ppm, δ), 10.40-10.16 (br, 2H, 2xNH), 7.70-7.14 (m, 9H, Aromatic protons), 6.67 (s, 1H, CH= in thiazole), 3.76-3.18 (p, 1H, methine proton in the Cyclobutane ring), 2.51-2.46 (m, 4H, CH_2 protons in Cyclobutane), 1.51 (s, 3H, CH_3 protons). $^{13}\text{C-NMR}$ (200 MHz, CDCl_3 , ppm), 178.21 (C=S, Cs), 163.11 (C-2 in Thiazole), 157.09 (Aromatic Quaternary C's), 153.81 (C-4 in Thiazole), 140.79, 131.41, 130.30, 127.84, 126.49, 125.47 (Aromatic C's), 106.56 (C-5) in Thiazole, 42.73, 40.93 (Cyclobutane (CH_2)₂ Cs), 32.61, (Cyclobutane CH); 32.03 (CH_3).

Computational Methods

Molecular geometry of the thiazole derivatives were obtained using the GaussView 5.0 package, which contains molecular imaging software that explains the geometry of molecules in the gas phase. Gaussian 09W software calculated the molecule structure [36, 37]. DFT is suitable for workstation capability in the Gaussian09W program at the basis set 6-311G(d,p). DFT is typically faster than Hartree-Fock techniques, with comparable results [38]. Larger basis sets should produce better and thus more

accurate results as they approach the infinite basis set limit. A constricted Gaussian basis set (6-311G) is generated for the ground states of first row atoms by optimizing exponents and coefficients at the Mo/lle-Plesset (MP) second-order level. There is a threefold split in the valence S and P shells, as well as a single set of uncontracted polarization functions, on each atom. The functions in parenthesis "(d)" or "(d,p)" are polarization functions, which are used to precisely define chemical bonds (higher angular momentum than the valence orbitals). Suppose there is no comma, as in (d). In that case, you are including polarization functions in all heavy atoms (except hydrogen). In contrast, if there is a comma (d,p), you include the first functions in heavy atoms and the second ones in hydrogen atoms [39].

DFT was used to calculate the electron density and other electronic properties of E_{HOMO} (higher occupational molecular orbital), E_{LUMO} (lowest occupational molecular orbital), ΔE (energy bandgap), (electronegativity) χ , (hardness) η , (softness) σ , (electrophilicity index) ω , (nucleophilicity index) ϵ , (Chemical potential) P_i , (dipole moment) μ , and (fraction of transferred electrons) ΔN . The HOMO, LUMO, and μ of the molecule are calculated in Gaussian from the output file, while other parameters are calculated using standard equations. The E_{HOMO} and E_{LUMO} values are correlated to their ionization energy and electron affinity values, according to Koopman's theorem [40, 41]. The following equations were used to calculate the other parameters:

$$I = -E_{\text{HOMO}} \quad [41] \quad (1)$$

$$A = -E_{\text{LUMO}} \quad [41] \quad (2)$$

$$\Delta E = (E_{\text{LUMO}} - E_{\text{HOMO}}) \quad [42] \quad (3)$$

$$\eta = (I - A) / 2 \quad [43] \quad (4)$$

$$\sigma = 1/\eta \quad [44] \quad (5)$$

$$\chi = (I + A) / 2 \quad [45] \quad (6)$$

$$P_i = -\chi \quad [45] \quad (7)$$

$$\omega = P_i^2 / 2\eta \quad [46] \quad (8)$$

$$\epsilon = P_i * \eta \quad [47] \quad (9)$$

The electrophilicity index (ω) (equation 8) was depleted as a result of electrons moving from transmitter to receiver. The nucleophilicity index (ϵ) (equation 9) is a new chemical structure identifier. (ΔN) represents the number of electrons exchanged between the inhibitor and the metal.

$$\Delta N = \frac{\chi_{\text{metal}} - \chi_{\text{inhibitor}}}{2(\eta_{\text{metal}} - \eta_{\text{inhibitor}})} \quad [48] \quad (10)$$

The χ inhibitor and η inhibitor values in the equation are determined theoretically, and Pearson [50] experimentally calculates the χ and η for metals. According to Pearson, η for

metal are zero, and ionization potential (I) with electron affinity (A) for a single metal is equal ($I = A$).

Results and Discussion

Spectroscopy Analysis

The theoretical vibrational frequencies for our products were predicted using B3LYP/6-311(d,p). The vibrational band assignments were used to create the molecular visualization. To encourage the assignment of the observed peaks, we measured the theoretical vibrational frequencies of thiazole

derivatives (IIIa and IIIb) and compared them to their experimental results, as shown in Figure 2. In general, the results of this study's experimental data and theoretical results are comparable. For both compounds, the N-H stretching vibration was observed in the 3280-3200 cm^{-1} range. For both compounds (IIIa and IIIb), the peak for ($\nu\text{C-H}$) in cycloalkane was detected at 3107 cm^{-1} . The ($\nu\text{C-H}$) vibration peaks for aromatic and aliphatic were observed at 3055, 2980-2870 cm^{-1} respectively. In both IIIa and IIIb derivatives of thiazol the peaks for ($\nu\text{C=N}$), ($\nu\text{C=S}$), ($\nu\text{C-N}$), ($\nu\text{C-S-C}$), were found in a range 1600-1590, 1360-1340, 1159-1000, 690-655 individually. In the FT-IR vibration analysis, there is no identical peaks were found between IIIa and IIIb. All FT-IR peaks for both derivatives are observed in very close ranges.

In $^1\text{H-NMR}$ spectra, the N-H proton peak for IIIa appeared at 10.46-10.06 ppm (br, 2H, 2xNH), while for IIIb was appeared at 10.40-10.16 ppm. Protons in aromatic (m, 9H, Aromatic protons) were found to be 7.55-7.12 ppm for IIIa,

and the same peaks for IIIb were found at 7.70-7.14 ppm. In the IIIa compound at 6.42 ppm, a single proton peak for thiazole was observed, while the same peak for IIIb was found at 6.67 ppm. The peaks for cyclobutane ring (p, 1H, methine proton in the), Cyclobutane (m, 4H, CH_2 protons in), and CH_3 protons (s, 3H,) in Derivative IIIa were observed at 3.73-3.60, 2.68-2.46, and 1.56 ppm, while the peaks for derivative IIIb was observed at 3.76-3.18, 2.51-2.46, and 1.51 ppm respectively.

In $^{13}\text{C-NMR}$ spectra, the Cs for C=S and C-2 for thiazole has been observed at 178.22, 163.11 ppm for compound IIIa, and compound IIIb has been observed at 178.21 and 163.11 ppm. For the derivatives IIIa and IIIb, the Aromatic Quaternary C's were found at 157 ppm. The (C-4) in Thiazole for both IIIa and IIIb were detected at 153.81 ppm. The peaks for (C-5) thiazole, (Cyclobutane (CH_2)₂ Cs), (Cyclobutane CH), and (CH_3) for IIIa were found at 106.56, 42.73, 40.93, 32.61, and 32.03, the same peaks for IIIb were detected at 106.56, 42.73, 40.93, 32.61, and 32.03 ppm.

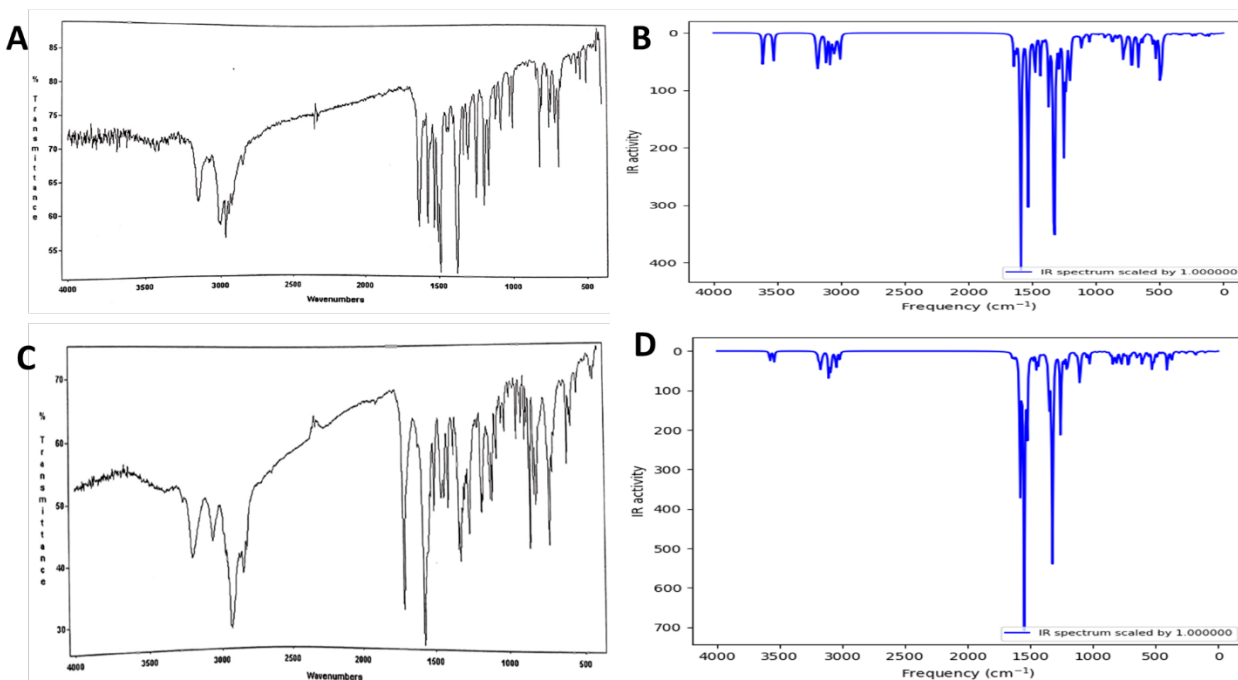


Fig. 2 Shows FT-IR spectra. a) Experimentally vibration for IIIa, b) Theoretically vibration for IIIa, c) Experimentally vibration for IIIb, d) Therotically vibration for IIIb.

Geometrical Optimization

Geometrical optimization for both derivatives (IIIa and IIIb) in the gas phase was investigated using B3LYP/6-311 (d,p). Figure 3 depicts the theoretical geometric structure of a molecular with assigned atomic number. Tables 1 and 2

show the bond length, bond angle, and dihedral angles for all non-hydrogen atoms. Normal mode analysis yielded no negative frequencies for any of the structures using any of the measurement methods.

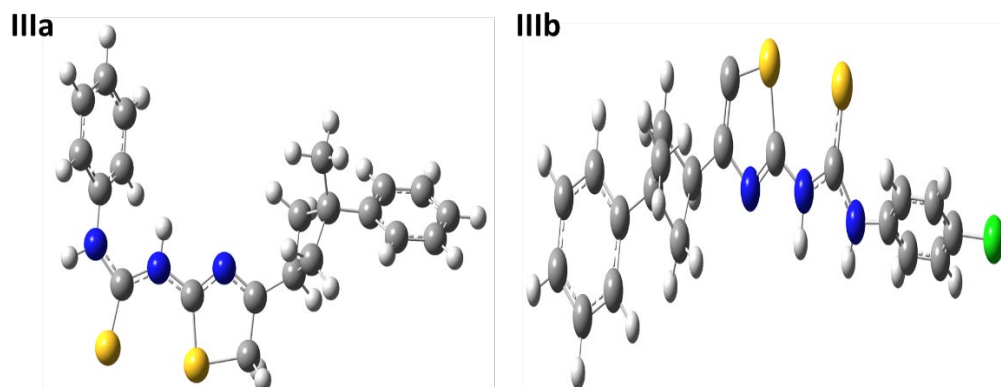


Fig. 3 Geometrical molecular optimization for IIIa and IIIb in the gas phase at the DFT/B3LYP theoretical stage using the 6-311G basis set (d,p).

Table 1. The geometrical optimization (Bond Length, Bond angle, and Dihedral angle) for the compound IIIa

Symbol	Bond Length	Symbol	Bond Angle	Symbol	Dihedral Angle
C2-C1	1.3932754	C3-C2-C1	121.2615898	C4-C3-C2-C1	0.8930745
C3-C2	1.4000661	C4-C3-C2	117.6993838	C5-C4-C3-C2	-0.913626
C4-C3	1.4004661	C5-C4-C3	121.2796904	C6-C1-C2-C3	-0.2445198
C5-C4	1.392962	C6-C1-C2	120.2580631	C12-C3-C2-C1	176.3404345
C6-C1	1.3924168	C12-C3-C2	121.1752472	C13-C12-C3-C2	42.2071615
C12-C3	1.5273235	C13-C12-C3	114.3412083	C14-C12-C3-C2	140.7611124
C13-C12	1.5652098	C14-C12-C3	113.9999358	C15-C13-C12-C3	97.9310952
C14-C12	1.5648552	C15-C13-C12	89.9844155	C21-C12-C12-C2	-88.6575988
C15-C13	1.5512068	C21-C12-C12	109.346835	C25-C15-C13-C12	139.50367
C21-C12	1.5348029	C25-C15-C13	119.3294972	C26-C25-C15-C13	153.3724144
C25-C15	1.4878166	C26-C25-C15	121.9992845	C27-C25-C15-C13	-34.6799438
C26-C25	1.5111412	C27-C25-C15	155.020296	N30-C27-C25-C15	6.9711263
C27-C25	2.2210611	N30-C27-C25	33.065307	S31-C27-C25-C15	-172.4119697
N30-C27	1.3234806	S31-C27-C25	83.6165019	N32-C27-C25-C15	10.8136106
S31-C27	1.773513	N32-C27-C25	150.2968174	N34-N32-C27-C15	171.5465661
N32-C27	1.3816223	N34-N32-C27	164.0608005	C36-N34-N32-C27	-160.7101018
N34-N32	2.3060429	C36-N34-N32	98.1403818	C37-C36-N34-N32	-133.5871373
C36-N34	1.4156939	C37-C36-N34	118.6312115	C38-C36-N34-N32	49.1515068
C37-C36	1.4007618	C38-C36-N34	122.0040889	C39-C37-C36-N34	-177.4883883
C38-C36	1.4018611	C39-C37-C36	120.2555121	C41-C38-C36-N34	178.5735886
C39-C37	1.3902426	C41-C38-C36	119.9232552	C43-C41-C38-C36	-1.337642
C41-C38	1.3924325	C43-C41-C38	120.6426911	C47-N32-C27-C25	178.6924332
C43-C41	1.3926764	C47-N32-C27	131.3513147	S48-C47-N32-C27	5.3208851
C47-N32	1.3633807	S48-C47-N32	125.1002754		
S48-C47	1.6765737				

Table 2. The geometrical optimization (Bond Length, Bond angle, and Dihedral angle) for the compound IIIb

Symbol	Bond Length	Symbol	Bond Angle	Symbol	Dihedral Angle
C2-C1	1.3930346	C3-C2-C1	121.0758826	C4-C3-C2-C1	0.3530461
C3-C2	1.3995549	C4-C3-C2	118.0744156	C5-C4-C3-C2	-0.3662822
C4-C3	1.3993615	C5-C4-C3	121.0545181	C6-C5-C4-C3	0.122452
C5-C4	1.3932813	C6-C5-C4	120.2161636	C12-C3-C2-C1	177.439137
C6-C5	1.3928901	C12-C3-C2	120.8136125	C13-C12-C3-C2	40.6237812

C12-C3	1.5179693	C13-C12-C3	116.5431953	C14-C12-C3-C2	143.4137268
C13-C12	1.5661138	C14-C12-C3	116.6740886	C15-C14-C12-C3	-129.2058108
C14-C12	1.5669021	C15-C14-C12	90.2796206	C21-C12-C3-C2	-87.8199518
C15-C14	1.5525618	C21-C12-C3	109.5992927	C25-C15-C14-C12	-112.9468478
C21-C12	1.5387035	C25-C15-C14	92.7354009	C26-C25-C15-C14	170.1145357
C25-C15	2.5748125	C26-C25-C15	26.6178702	C27-C26-C25-C15	179.3562494
C26-C25	1.3505699	C27-C26-C25	78.6622125	N28-C27-C26-C25	179.9855619
C27-C26	2.2425399	N28-C27-C26	34.9481401	S29-C25-C15-C14	170.7934498
N28-C27	1.303682	S29-C25-C15	141.5091587	N30-C27-C26-C25	179.6476029
S29-C25	1.7423714	N30-C27-C26	152.7249233	C32-N30-C27-C26	178.9995887
N30-C27	1.3899947	C32-N30-C27	130.7760881	S33-C32-N30-C27	4.3983195
C32-N30	1.3727767	S33-C32-N30	123.3153105	N34-C32-N30-C27	-175.107688
S33-C32	1.6669766	N34-C32-N30	111.0081578	C36-N34-C32-N30	-176.0959425
N34-C32	1.3756074	C36-N34-C32	129.0500082	C37-C36-N34-C32	43.3535032
C36-N34	1.4165355	C37-C36-N34	122.6120502	C38-C35-N34-C32	-140.2152539
C37-C36	1.3974156	C38-C35-N34	117.883942	C39-C37-C36-C34	177.0155294
C38-C35	1.3978317	C39-C37-C36	120.0027956	C41-C38-C36-C34	-176.4920062
C39-C37	1.3899143	C41-C38-C36	120.7562013	C43-C41-C38-C36	-0.6530176
C41-C38	1.3902565	C43-C41-C38	119.1430957	C146-C43-C41-C38	-179.5618352
C43-C41	1.3895955	C146-C43-C41	119.5756551		
C146-C43	1.7580732				

Inhibitor Activity

Table 3 summarizes the HOMO and LUMO energies level. The HOMO and LUMO energy level for derivative IIIa, has greater than derivative III b. HOMO is associated with the ability to donate electrons and is required for the studding of corrosion. It can be seen that as HOMO values increase, so do the inhibitor molecules on the metal surface increase [49]. As a result, research on the mechanism of charge transfer on the metal surface and adsorption was permitted. Based on the high E_{HOMO}, derivative IIIa has the highest inhibitory activity compared to derivative IIIb which has the lowest inhibitory activity (lower E_{HOMO}). The level of the electron and its ability to accept electrons is referred to as LUMO. Reduced E_{LUMO} values indicate that the inhibitor molecule adds an extra negative charge to the metal's surface. The LUMO energy level for Both IIIa and IIIb were more different from each other. It was also discovered that the energy of HOMO and LUMO for inhibitor molecules is higher; as a result, the derivative IIIa inhibitors were

discovered to be reactive by acting as a donor (no Halogen groups) and anti-corrosion activity. The derivative IIIb inhibitor has the lowest E_{HOMO} and E_{LUMO} values, minimizing metal reactivity and metal donor electrons to the inhibitor. The inhibitor activity has decreased, while the metal's reactivity has increased. According to HOMO-LUMO capacity, Derivative IIIa has the most powerful corrosion inhibition. The energy gap between E_{HOMO} and E_{LUMO} is important for calculating theoretical inhibitory efficiency for molecular reactivity. It is useful for inhibitor studies to compare ΔE between the two derivatives. The shorter the energy distances, the greater the efficiency of inhibition. The lower value of ΔE in corrosion inhibitors is based on E_{HOMO} rather than E_{LUMO}. Inhibitor derivatives with high HOMO and low ΔE can be used as effective anti-corrosion agents [50]. Because of the increased HOMO energy value and decreasing ΔE, it can be concluded that derivative IIIa would have an intense inhibitory activity, as shown in Figure 4.

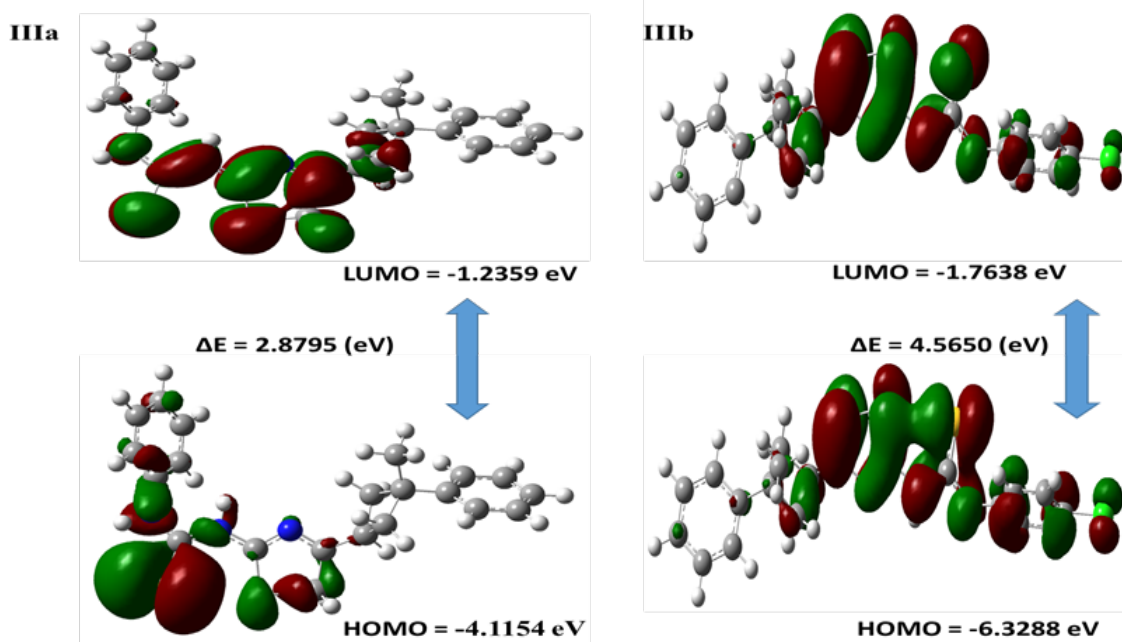


Fig. 4 HOMO and LUMO diagram for IIIa and IIIb

Table 3. Calculated electron identifier using B3LYP/6-311G(d,p) for IIIa and IIIb

Parameters	Equations	IIIa	IIIb
Total Energy (a.u)		-1774.365	-2232.712
μ (D)		4.569	3.973
E_{LUMO} (eV)		-1.235950872	-1.763855912
E_{HOMO} (eV)		-4.115482384	-6.328873928
ΔE (eV)		2.879531512	4.565018016
I	$I = -E_{HOMO}$	4.115482384	6.328873928
A	$A = -E_{LUMO}$	1.235950872	1.763855912
χ (eV)	$\chi = (I + A) / 2$	2.675716628	4.04636492
η (eV)	$\eta = (I - A) / 2$	1.439765756	2.282509008
σ (eV)	$\sigma = 1/\eta$	0.694557428	0.438114372
P_i (eV)	$P_i = \chi$	-2.675716628	-4.04636492
ω (eV)	$\omega = P_i^2/2\eta$	2.486327878	3.586638434
ε (eV)	$\varepsilon = P_i \cdot \eta$	-3.852405174	-9.23586438
ΔN	$\Delta N = (\chi_{\text{metal}} - \chi_{\text{inhibitor}}) / 2, (\eta_{\text{metal}} - \eta_{\text{inhibitor}})$	1.501731568	0.647014989

Figure 5 shows the charges on the atoms of the derivative's molecular structure. Mulliken methods are widely used to estimate inhibitor adsorption sites. Many researchers have argued that the presence of heteroatoms as a result of the donor-acceptor process has improved the ability to adsorb on

the metal surface [51]. Because of the negatively charged atoms such as N, O, and C atoms in the aromatic ring, derivative IIIa has a more effective inhibitory than derivative IIIb, see Figure 5.

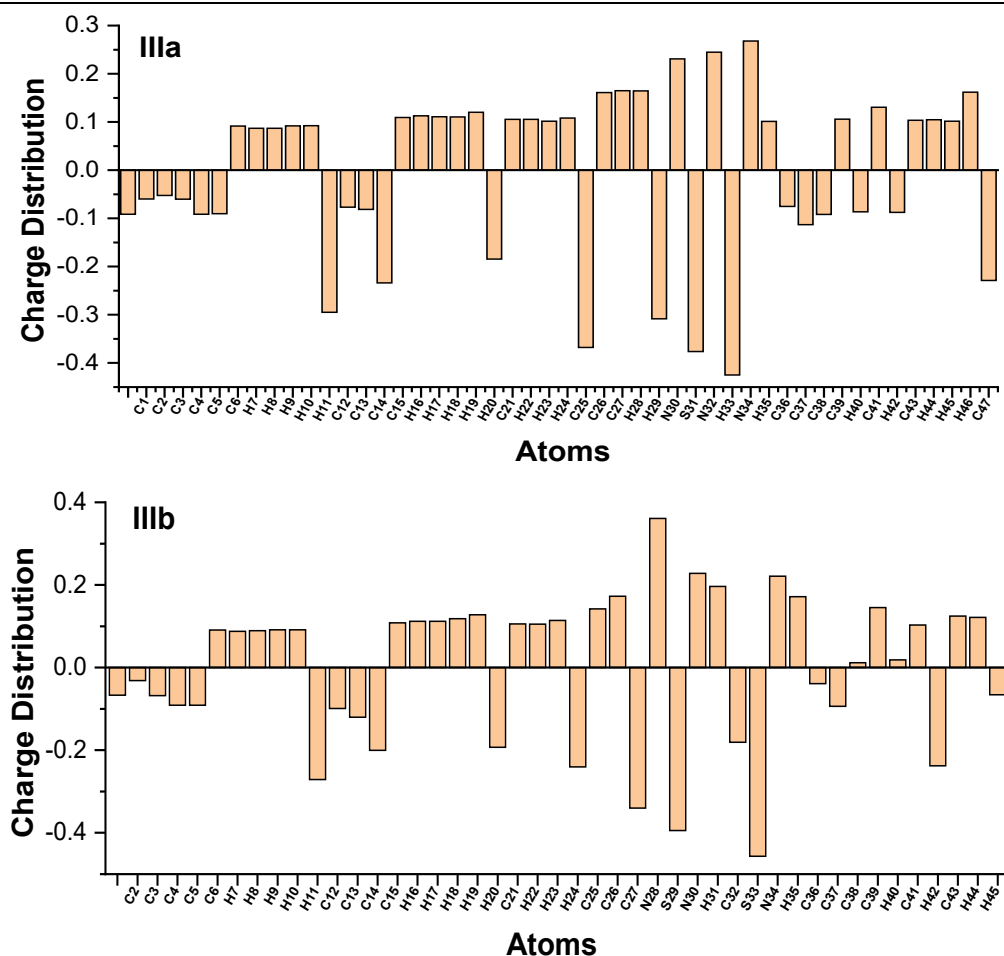


Fig. 5 Charge distribution on the atoms for both IIIa and IIIb.

Other parameters that can be used to determine an inhibitor's stability, reactivity, and inhibitor activity are η and σ . The σ was greater for derivative IIIa than for derivative IIIb, as shown in Table 3. Because the organic inhibitor used is lewis-based, and soft inhibitors are more reactive than hard inhibitors, they are more effective corrosion inhibitors. The derivative IIIa inhibits with a high E_{HOMO} and a low ΔE , its estimated softness values to be high. The η and σ values have stronger inhibitory effects on derivative IIIa than on derivative IIIb.

The parameters χ and P_i are also used to assess inhibitor activity. The calculated inhibitor, χ values explain how the metal and the inhibitor form a coordinated covalent bond. The corrosion inhibition behavior of iron metal on the inhibitor derivatives. The χ values of the inhibitors in Table 3 were discovered to be less than the value of the iron metal. The iron metal was able to form bonds by absorbing electrons from the inhibitor molecule. The inhibition of derivative IIIa had a lower value of χ and served as the most effective corrosion inhibitor.

Table 3 summarizes the dipole moment (μ) data. According to the literature, there is no direct relationship between μ and inhibition activity. In some studies, the activity of molecules increased with increasing μ value, whereas in others, the inhibition molecule's activity decreased with increasing μ value. The derivative IIIa inhibitor has a higher dipole

moment, which can be perceived as a better covering on a metal surface.

The ω and ε are important parameters for determining inhibitors to corrosion activities. The ω shows the ability of the inhibitor molecules to accept electrons and ε the ability of the inhibitor molecules to donate electrons. Inhibitory activity increases as the ε value increases and decreases as the value of ω decreases [52]. In the derivatives of IIIa and IIIb, the ε increase in derivatives IIIa and ω has lower than derivative IIIb. Derivative IIIa has a stronger inhibitory effect than derivative IIIb based on ω and ε parameters. The ΔN values of derivative IIIa indicate that it is a good inhibitor because the value was greater than derivative IIIb, implying that more electrons are transferred from organic compound IIIa to the surface of iron metals.

Conclusion

In the first step of this research, new thiazole derivatives (IIIa, b) were synthesized by activating two different isothiocyanate (II) RNCS compounds with 4-(1-Phenyl-1-methyl-cyclobutane-3-yl)-2-aminithiazole (I). Their molecular structures were determined using IR, 1H , and ^{13}C -NMR techniques. According to the results, compound IIIa has a higher E_{HOMO} and E_{LUMO} value than compound IIIb. As a result, compound IIIa was determined to be a good donor with high inhibitor activity. Because of the lower ΔE of the compound IIIa has a stronger inhibitory activity.

Furthermore, because it has a higher dipole moment value of IIIa, it can improve metal corrosion resistance. Based on the atomic charges of the compound, it was discovered that the electronegative atoms have a significant influence on the inhibition action. The atomic charge distribution in derivative IIIa suggests that electronegative atoms significantly impact inhibitory activity. The determined parameters, including η , ω , σ , ϵ , P_i and χ showed that compound IIIa has a strong corrosion inhibitor effect. A lower inhibitor value suggests that the iron metal can form a bond by absorbing electrons from the compound inhibitor. The higher the ΔN value, the better the metal surface can be adsorbed, and increasing corrosion inhibition. Finally, both compounds appear to be promising anti-corrosion agents. The complexity of organic structures and increased number of heteroatoms for both derivatives are effective corrosion inhibitors.

References

- R. Omar, P. Koparir, and M. Koparir, Synthesis of 1, 3-Thiazole derivatives. *Indian Drugs*, 2021. 1: p. 58.
- A. Cansiz, et al., Synthesis of tautomeric forms of 5-(2-hydroxyphenyl)-4-substituted-3H-1, 2, 4-triazole-3-thione. *Asian Journal of Chemistry*, 2009. 21(1): p. 617.
- P. Koparir, et al., Synthesis and in-vitro antimicrobial activity of novel aminophosphinic acids containing cyclobutane and 1, 3-thiazole. *Phosphorus, Sulfur, and Silicon and the Related Elements*, 2011. 186(12): p. 2368-2376.
- A.R. Sayed and J.S. Wiggins, 1, 3-Dipolar cycloaddition polymerization reactions of novel macromolecules containing sym-tetrazine rings. *Polymer*, 2008. 49(9): p. 2253-2259.
- A.V. Moradi, et al., Theoretical study of thiazole adsorption on the (6, 0) zigzag single-walled boron nitride nanotube. *Bulletin of the Korean Chemical Society*, 2012. 33(10): p. 3285-3292.
- S.H. Ali and A.R. Sayed, Review of the synthesis and biological activity of thiazoles. *Synthetic Communications*, 2021. 51(5): p. 670-700.
- X.-X. Xie, et al., Synthesis and anticancer effects evaluation of 1-alkyl-3-(6-(2-methoxy-3-sulfonylaminopyridin-5-yl) benzo [d] thiazol-2-yl) urea as anticancer agents with low toxicity. *Bioorganic & Medicinal Chemistry*, 2015. 23(19): p. 6477-6485.
- A. Prakash and D. Adhikari, Application of Schiff bases and their metal complexes-A Review. *Int. J. Chem. Tech. Res*, 2011. 3(4): p. 1891-1896.
- W. Zopubi, Biological activities of Schiff bases and their complexes: a review of recent work. *Int. J. Org. Chem*, 2013. 3: p. 73-95.
- H. Kunkely and A. Vogler, Photochemistry of N, N'-bis (3, 5-di-tert-butylsalicylidene)-1, 2-diaminocyclohexane and its Co (II) complex in chloroform. *Journal of Photochemistry and Photobiology A: Chemistry*, 2001. 138(1): p. 51-54.
- S.H. Rahaman, et al., Synthesis, structure and properties of mononuclear cobalt (II) and cobalt (III) pseudohalide complexes containing N-donor Schiff bases: Synthetic control of metal oxidation levels. *Polyhedron*, 2005. 24(13): p. 1755-1763.
- N. Gümrükçüoğlu, et al., Determination of stability constants of triazole ligand carrying naphthol group with heavy metal ions in aqueous solutions. *Pakistan Journal of Analytical & Environmental Chemistry*, 2013. 14(2): p. 7.
- J. Li, et al., Recent advances in the total synthesis of cyclobutane-containing natural products. *Organic Chemistry Frontiers*, 2020. 7(1): p. 136-154.
- P. Koparir, et al., Elucidation of Potential Anticancer, Antioxidant and Antimicrobial Properties of Some New Triazole Compounds Bearing Pyridine-4-yl Moiety and Cyclobutane Ring. *Arabian Journal of Chemistry*, 2022: p. 103957.
- V.M. Dembitsky, Naturally occurring bioactive Cyclobutane-containing (CBC) alkaloids in fungi, fungal endophytes, and plants. *Phytomedicine*, 2014. 21(12): p. 1559-1581.
- P. KOPARIR, et al., Synthesis, Characterization, and theoretical inhibitor study for (1E, 1'E)-2, 2'-thiobis (1-(3-mesityl-3-methylcyclobutyl) ethan-1-one) dioxime. *El-Cezeri*, 2020. 8(3): p. 1495-1510.
- T. Seiser, et al., Cyclobutanes in catalysis. *Angewandte Chemie International Edition*, 2011. 50(34): p. 7740-7752.
- R. Sure and S. Grimme, Corrected small basis set Hartree-Fock method for large systems. *Journal of computational chemistry*, 2013. 34(19): p. 1672-1685.
- L. Türker, et al., A DFT study on nitrotriazines. *Journal of Hazardous Materials*, 2009. 167(1-3): p. 440-448.
- R.A. OMER, et al., Computational and spectroscopy study of melatonin. *Indian Journal of Chemistry-Section B (IJC-B)*, 2021. 60(5): p. 732-741.
- O. Rebaz, et al., Theoretical Determination of Corrosion Inhibitor Activities of Naphthalene and Tetralin. *Gazi University Journal of Science*: p. 1-1.
- R.A. Omer, et al., Theoretical analysis of the reactivity of chloroquine and hydroxychloroquine. *Indian Journal of Chemistry-Section A (IJCA)*, 2020. 59(12): p. 1828-1834.
- P. Koparir, et al., Theoretical determination of corrosion inhibitor activities of 4-allyl-5-(pyridin-4-yl)-4H-1, 2, 4-triazole-3-thiol-thione tautomerism. 2022.
- X. Li, S. Deng, and H. Fu, Three pyrazine derivatives as corrosion inhibitors for steel in 1.0 M H₂SO₄ solution. *Corrosion science*, 2011. 53(10): p. 3241-3247.
- P. Koparir, K. Sarac, and R.A. Omar, Synthesis, molecular characterization, biological and computational studies of new molecule contain 1, 2, 4-triazole, and Coumarin bearing 6, 8-dimethyl. *Biointerface Research in Applied Chemistry*, 2022. 12(1): p. 809-823.
- J. Fang and J. Li, Quantum chemistry study on the relationship between molecular structure and corrosion inhibition efficiency of amides. *Journal of Molecular Structure: THEOCHEM*, 2002. 593(1-3): p. 179-185.
- O. Rebaz, et al., Computational determination the reactivity of salbutamol and propranolol drugs. *Turkish Computational and Theoretical Chemistry*, 2020. 4(2): p. 67-75.

28. L. AHMED and O. Rebaz, 1H-Pyrrole, Furan, and Thiophene Molecule Corrosion Inhibitor Behaviors. *Journal of Physical Chemistry and Functional Materials*, 4(2): p. 1-4.
29. L. AHMED and O. Rebaz, Computational Study on Paracetamol Drug. *Journal of Physical Chemistry and Functional Materials*, 2020. 3(1): p. 9-13.
30. L.A. OMER and R.O. ANWER, Population Analysis and UV-Vis spectra of Dopamine Molecule Using Gaussian 09. *Journal of Physical Chemistry and Functional Materials*, 2020. 3(2): p. 48-58.
31. L.J. Bartolotti and K. Flurhick, An introduction to density functional theory. *Reviews in computational chemistry*, 1996. 7: p. 187-260.
32. L. AHMED and O. Rebaz, Spectroscopic properties of Vitamin C: A theoretical work. *Cumhuriyet Science Journal*, 2020. 41(4): p. 916-928.
33. O. Rebaz, et al., Structure reactivity analysis for Phenylalanine and Tyrosine. *Cumhuriyet Science Journal*, 2021. 42(3): p. 576-585.
34. R.A. Omer, P. Koparir, and L.O. Ahmed, Characterization and Inhibitor Activity of Two Newly Synthesized Thiazole. *Journal of Bio-and Triboro-Corrosion*, 2022. 8(1): p. 1-12.
35. M.G.K. AlFalah and F. Kandemirli, Corrosion inhibition potential of dithiohydrazodicarbonamide derivatives for mild steel in acid media: synthesis, experimental, DFT, and Monte Carlo studies. *Arabian Journal for Science and Engineering*, 2021: p. 1-30.
36. R. Dennington, T. Keith, and J. Millam, GaussView, version 5. 2009.
37. L. AHMED and O. Rebaz, The Role of the Various Solvent Polarities on Piperine Reactivity and Stability. *Journal of Physical Chemistry and Functional Materials*. 4(2): p. 10-16.
38. A.D. Becke, Density-functional thermochemistry. IV. A new dynamical correlation functional and implications for exact-exchange mixing. *The Journal of chemical physics*, 1996. 104(3): p. 1040-1046.
39. D. Bálint and L. Jäntschi, Comparison of molecular geometry optimization methods based on molecular descriptors. *Mathematics*, 2021. 9(22): p. 2855.
40. T. Koopmans, Über die Zuordnung von Wellenfunktionen und Eigenwerten zu den einzelnen Elektronen eines Atoms. *physica*, 1934. 1(1-6): p. 104-113.
41. B.N. Plakhutin and E.R. Davidson, Koopmans' Theorem in the Restricted Open-Shell Hartree– Fock Method. 1. A Variational Approach. *The Journal of Physical Chemistry A*, 2009. 113(45): p. 12386-12395.
42. E.P. Jesudason, et al., Synthesis, pharmacological screening, quantum chemical and in vitro permeability studies of N-Mannich bases of benzimidazoles through bovine cornea. *European journal of medicinal chemistry*, 2009. 44(5): p. 2307-2312.
43. H. Gökce and S. Bahceli, A study on quantum chemical calculations of 3-, 4-nitrobenzaldehyde oximes. *Spectrochimica Acta Part A: Molecular and Biomolecular Spectroscopy*, 2011. 79(5): p. 1783-1793.
44. M. Arivazhagan and V. Subhasini, Quantum chemical studies on structure of 2-amino-5-nitropyrimidine. *Spectrochimica Acta Part A: Molecular and Biomolecular Spectroscopy*, 2012. 91: p. 402-410.
45. M.S. Masoud, et al., Synthesis, computational, spectroscopic, thermal and antimicrobial activity studies on some metal–urate complexes. *Spectrochimica Acta Part A: Molecular and Biomolecular Spectroscopy*, 2012. 90: p. 93-108.
46. S.-i. Kiyooka, D. Kaneno, and R. Fujiyama, Parr's index to describe both electrophilicity and nucleophilicity. *Tetrahedron Letters*, 2013. 54(4): p. 339-342.
47. R.G. Pearson, Absolute electronegativity and hardness: application to inorganic chemistry. *Inorganic chemistry*, 1988. 27(4): p. 734-740.
48. A.Y. Musa, R.T. Jalgham, and A.B. Mohamad, Molecular dynamic and quantum chemical calculations for phthalazine derivatives as corrosion inhibitors of mild steel in 1 M HCl. *Corrosion Science*, 2012. 56: p. 176-183.
49. S. Chen, et al., Quantum chemical study of some benzimidazole and its derivatives as corrosion inhibitors of steel in HCl solution. *Int. J. Electrochem. Sci*, 2014. 9: p. 5400-5408.
50. M. Beytur, et al., Synthesis, characterization and theoretical determination of corrosion inhibitor activities of some new 4, 5-dihydro-1H-1, 2, 4-Triazol-5-one derivatives. *Heliyon*, 2019. 5(6): p. e01809.
51. Z. El Adnani, et al., DFT theoretical study of 7-R-3methylquinoxalin-2 (1H)-thiones (RH; CH₃; Cl) as corrosion inhibitors in hydrochloric acid. *Corrosion Science*, 2013. 68: p. 223-230.
52. N. Karakus and K. Sayin, The investigation of corrosion inhibition efficiency on some benzaldehyde thiosemicarbazones and their thiole tautomers: Computational study. *Journal of the Taiwan Institute of Chemical Engineers*, 2015. 48: p. 95-102.